

Finding Golgi Stacks in Electron Micrographs

Neil Fordyce¹

neilfordyce@hotmail.com

Stephen McKenna¹

stephen@computing.dundee.ac.uk

Christian Hacker²

ch84@st-andrews.ac.uk

John Lucocq²

jml7@st-andrews.ac.uk

¹ School of Computing

University of Dundee

Dundee, UK

² School of Medicine

University of St Andrews

St Andrews, UK

Abstract

Transmission electron microscopy (EM) can acquire images in which a range of sub-cellular organelles are clearly resolved simultaneously. There exist mature stereology techniques for extracting quantitative specimen information from section-based EM images and such techniques have been adopted successfully for use in immuno-EM. A bottleneck preventing the application of these nanomorphomics methods to high throughput applications is the recognition of organelle structures. This paper addresses this issue for one important organelle, the Golgi apparatus. A support vector machine is trained as a local Golgi detector based on rotationally invariant features. The SVM output is used to drive a graph-cuts segmentation. The ability of the method to detect and segment Golgi stacks is evaluated on a set of 36 micrographs.

1 Introduction

Transmission electron microscopy (EM) can acquire images in which a range of organelles and their substructures are clearly resolved simultaneously. Furthermore, there exist mature stereology techniques for extracting quantitative specimen information from section-based EM images, providing unbiased and efficient estimates of 3D volumes, surfaces, and numbers as well as the distributions of organelles (e.g. [9]). Such techniques have been adopted successfully for use in immuno-EM, a method that maps molecular components and their concentrations over a range of subcellular compartments using particulate nanogold markers [10]; detection of the nanogold markers can be automated [16]. A bottleneck preventing the application of these *nanomorphomics* methods to high throughput data mining is the recognition of organelle structures in the images, a task which is carried out by trained experts. This paper addresses the automatic recognition and segmentation of one important organelle, the Golgi apparatus. The Golgi apparatus includes a stack of flat membrane-bound structures called cisternae. This stack usually presents visually in section as repeating curvilinear structures. Vesicles can often be seen in proximity to the stack. Figure 1(a) shows

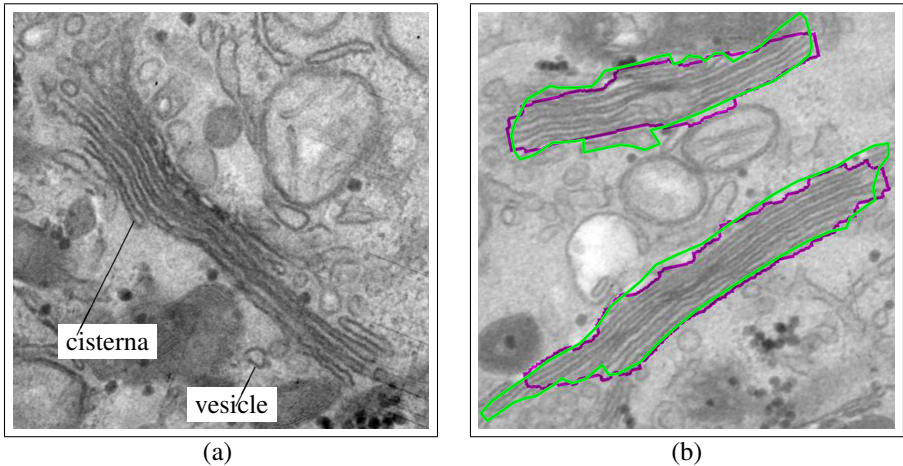


Figure 1: EM micrograph images cropped to 2000x2000 pixels. (a) Golgi apparatus with its stack of cisternae. (b) Manual (green) and automatic (magenta) segmentations.

an electron micrograph in which Golgi apparatus is clearly visible. In Figure 1(b), manual annotations of the extent of Golgi stacks are overlaid, along with a segmentation obtained automatically using the method described in this paper.

2 Related Work

We are not aware of any previous literature on automatic recognition of Golgi apparatus in EM images. There is however published work regarding other organelles and structures. For example, progress has been made on segmentation of mitochondria [2, 12, 13]. Perhaps most promisingly, Lucchi et al. [8] segmented mitochondria from surrounding background using support vector machine classifiers to assign probabilities to superpixels based on local texture and shape descriptors that were then used in a graph cuts optimization. A similar approach was applied to FIBSEM image stacks [9].

Regarding other structures, Nam et al. [10] segmented secretory granules using level set active contours and membrane sampling. Kreshuk et al. [5] detected synapses in intact nervous tissue in a FIBSEM image by training a random forest classifier to classify voxels based on local features. Others have presented methods for automatic enhancement and localisation of thin elongated structures in EM images [1, 14, 15].

3 Method

Firstly, a detection stage uses an SVM detector trained on subwindows of EM images. The detector uses features based on Histogram of Oriented Gradients (HOG). These features extend standard HOG to provide rotation-invariant Fourier HOG [7] descriptors. The key idea is treating gradient histograms as continuous functions, analysing polar coordinate gradient images in Fourier space. The features are the same regardless of the orientation of the Golgi stack which is arbitrary. Due to noise from the image acquisition technique, robustness to

noise is also desirable. Fourier HOG features offer both of these characteristics. The first three degrees of Fourier basis are used for the Fourier representation. The feature vector for each window comprises of 78 real-valued features. A binary SVM is trained on features extracted from hand annotated images, to discriminate between Golgi and non-Golgi sub-windows. Each sampled feature vector describes a subwindow of the image. Using a sliding window approach, the SVM is used to obtain an SVM score image which forms the output of the detection stage.

Secondly, graph cuts is used to produce segmentations by combining the detector output with spatial information from the original EM image. We use a graph cuts library [14] which implements approximate energy minimisation techniques. As in [9], our energy function, E , of a labelling, L , can be expressed as

$$E(L) = \sum D_p(L_p) + \lambda \sum V_{p,q}(L_p, L_q) \quad (1)$$

where λ is a parameter that determines the relative importance of a spatially coherent segmentation to one which is consistent with the results of the detection stage. D is a data cost w.r.t. the SVM probability image. It penalises assignment of pixels to labels with SVM scores inconsistent with other SVM scores in that labelling. Specifically, the data cost of assigning a label L_p to a pixel with SVM score s_p , is given by Equation (2) where μ_L and σ_L^2 are the mean and variance, respectively, of SVM scores of pixels assigned to label L .

$$D_p(L_p) = \frac{(s_p - \mu_L)^2}{\sigma_L^2} \quad (2)$$

V penalises crossing gradient boundaries in the EM image and encourages a smooth final segmentation which adheres to image contours. For adjacent pairs of pixels I_p and I_q , labelled L_p and L_q respectively, we have:

$$V_{p,q}(L_p, L_q) = \begin{cases} \exp(-|I_p - I_q|) & \text{if } L_p \neq L_q \\ 0 & \text{otherwise} \end{cases} \quad (3)$$

As a final step, any segmented components with an area below a threshold are removed.

4 Experiments

Our data set consisted of 36 electron micrographs of rabbit kidney cells. Each image had a resolution of 4725×4167 pixels. Images were subsampled to 945×834 pixels for feature extraction and the detector window size was then 31×31 pixels.

The Golgi stacks in the dataset were of various shapes and sizes. Some were very clearly defined and in focus, while other stacks appeared blurred and were identifiable in part due to proximal vesicles. All Golgi stacks were segmented manually to provide ground truth. Golgi which were badly blurred were given an additional annotation of *blurred*. Two sets of results are presented: one in which all Golgi were required to be detected, the other in which blurred Golgi were discounted.

Five-fold cross-validation was used to train and test detectors. The Fourier HOG features create densely populated descriptors for each image. 7200 negative and 9600 positive training examples were extracted at random from the training images to train an SVM.

Figure 2 shows example Golgi images with automatic segmentations overlaid, as well as the corresponding SVM outputs. Figure 2(b) shows two segmentation attempts: one of

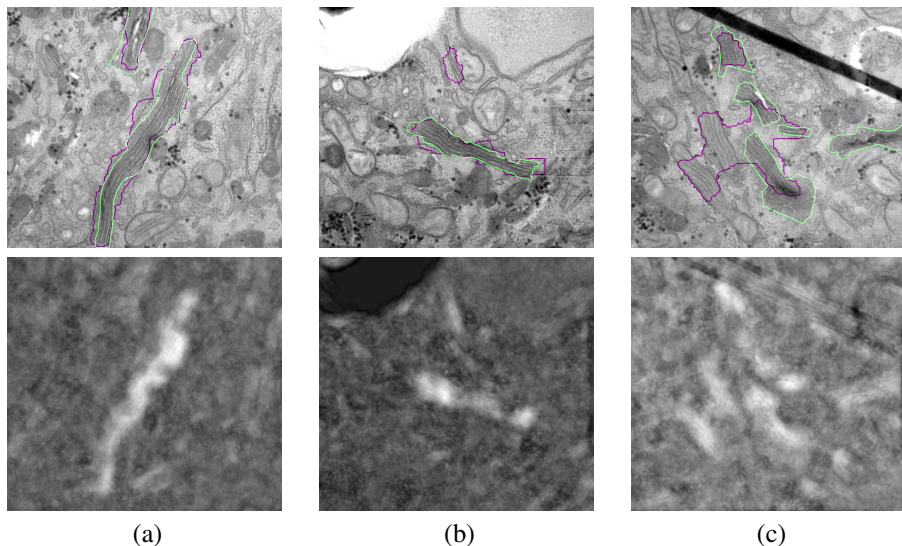


Figure 2: Top row: manual (green) and automatic (magenta) segmentations of Golgi stacks. Bottom row: SVM detector score images used as input to the graph cuts segmentation.

these is a reasonable segmentation, while the other is a false segmentation caused by the membranes of several other organelles being aligned to appear similar to Golgi. Figure 2(c) shows two segmented regions: one of these is reasonable, the other contains parts of three separate Golgi stacks and nearby mitochondria. The mitochondria in the segmentation have an appearance resembling Golgi cisternae. The proximity of multiple Golgi and mitochondria have brought about a single large segmentation. The blurred appearance of another Golgi in 2(c) has caused it to be missed.

Figure 3 shows an ROC curve obtained by varying the SVM score threshold. The F1 score (F-measure) was 0.3157 (0.3235 when blurred Golgi were excluded); this low score arose from a high false positive rate; however, the false positives are often spatially isolated so are subsequently removed by graph cuts. The optimal pixel misclassification rate obtained was 0.1589 and this reduced to 0.0983 when blurred Golgi regions were excluded.

A Jaccard index was used to quantify the quality of segmentation as follows. A binary labelling L and binary ground truth G can be combined to produce an evaluation image $I = G + 2L$. A Jaccard index is obtained for each connected region R of non-zero pixels in I . So $p \in R \Rightarrow I(p) > 0$. Let $A = \{p | p \in R, I(p) = 3\}$ and let $B = \{p | p \in R, I(p) \geq 1\}$. Then the Jaccard index is defined for each R as, $J = \frac{|A \cap B|}{|A \cup B|}$. If multiple distinct Golgi regions are labelled as a single region, then the regions are evaluated as a single segmentation. If a single Golgi region is labelled with multiple segmentations, then the region is evaluated as a single segmentation. A schematic of this is shown in Figure 4; although one labelling contains multiple Golgi and one Golgi is labelled in parts, the entire region (red, green and blue) is counted as a single segmentation and assigned a single Jaccard index. If a Golgi region does not intersect with any region labelled as Golgi, this is counted as a missed segmentation. On the other hand, if a region labelled as Golgi does not intersect with any Golgi, this is counted as a false segmentation.

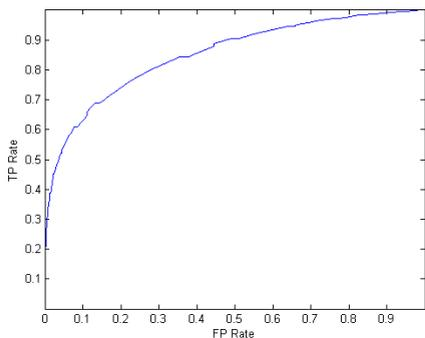


Figure 3: ROC curve (pixel classification)

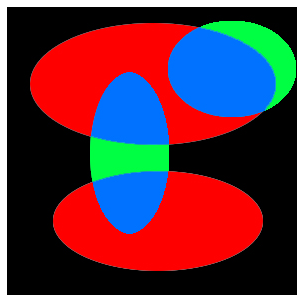


Figure 4: Segmentation schematic: Red=missed Golgi, green=incorrectly labelled Golgi, blue=correctly labelled Golgi, black=correctly labelled non-Golgi

	Inc. blur	Exc. blur
True detections	40	35
False detections	10	10
Missed Golgi	20	5

Table 1: Golgi detection results (including and excluding blurred Golgi regions)

Table 1 summarises segmentation results (with and without blurred regions). Although the number of missed Golgi was quite high, the majority of these came from blurred regions. The number of true detections dropped when blurred regions were excluded, indicating that some blurred Golgi had been detected. The mean Jaccard index across the true detections was 0.58 when blurred Golgi were included and 0.63 when they were excluded.

5 Conclusion

This paper contributes to the goal of automating organelle recognition in EM by demonstrating automatic detection and segmentation of Golgi stacks. High scoring segmentations occurred when Golgi stacks were in focus and some distance from other organelles. False segmentations largely arose from mitochondria and aligned membranes which appeared similar to Golgi. The majority of missed segmentations were of Golgi which were badly blurred. Considering vesicles associated with the Golgi stack could improve performance in these areas.

References

[1] S. Bagon. Matlab wrapper for graph cuts, December 2006. URL <http://www.wisdom.weizmann.ac.il/~bagon>.

[2] C. Bazán, M. Miller, and P. Blomgren. Structure enhancement diffusion and contour

- extraction for electron tomography of mitochondria. *J. Structural Biology*, 166(2): 144–155, 2009.
- [3] Y. Boykov and V. Kolmogorov. An experimental comparison of min-cut/max-flow algorithms for energy minimization in vision. *IEEE Trans. PAMI*, 26(9):1124–1137, 2004.
- [4] M. Jiang, Q. Ji, and B. F. McEwen. Automated extraction of fine features of kinetochore microtubules and plus-ends from electron tomography volume. *IEEE Transactions on Image Processing*, 15(7):2035–2048, 2006.
- [5] A. Kreshuk, C. N. Straehle, C. Sommer, U. Koethe, M. Cantoni, G. Knott, and F. A. Hamprecht. Automated detection and segmentation of synaptic contacts in nearly isotropic serial electron microscopy images. *PLoS One*, 6(10):e24899, 2011.
- [6] S. L. B. Kristiansen and J. R. Nyengaard. Digital stereology in neuropathology. *APMIS*, 120(4):327–340, 2012.
- [7] K. Liu, H. Skibbe, T. Schmidt, T. Blein, K. Palme, T. Brox, and O. Ronneberger. Rotation-invariant HOG descriptors using Fourier analysis in polar and spherical coordinates. *Int. J. Computer Vision*, 106(3):342–364, 2014.
- [8] A. Lucchi, K. Smith, R. Achanta, V. Lepetit, and P. Fua. A fully automated approach to segmentation of irregularly shaped cellular structures in EM images. In *Proc. MICCAI*, volume LNCS 6362, 2010.
- [9] A. Lucchi, K. Smith, R. Achanta, G. Knott, and P. Fua. Supervoxel-based segmentation of mitochondria in EM image stacks with learned shape features. *IEEE Transactions on Medical Imaging*, 30(11), 2011.
- [10] J. Lucocq. Quantification of structures and gold labeling in transmission electron microscopy. *Methods in Cell Biology*, 88:59, 2008.
- [11] D. Nam, J. Mantell, D. Bull, P. Verkade, and A. Achim. A novel framework for segmentation of secretory granules in electron micrographs. *Medical Image Analysis*, 18(2):411 – 424, 2014.
- [12] R. Narasimha, H. Ouyang, A. Gray, S. McLaughlin, and S. Subramaniam. Automatic joint classification and segmentation of whole cell 3D images. *Pattern Recognition*, 42(6):1067 – 1079, 2009.
- [13] H. Nguyen and Q. Ji. Shape-driven three-dimensional watersnake segmentation of biological membranes in electron tomography. *IEEE Trans. Medical Imaging*, 27(5): 616–628, 2008.
- [14] D. Nurgaliev, T. Gatanov, and D. J. Needleman. Automated identification of microtubules in cellular electron tomography. In *Microtubules: in vivo*, volume 97 of *Methods in Cell Biology*, pages 475 – 495. Acad. Press, 2010.
- [15] K. Sandberg and M. Brega. Segmentation of thin structures in electron micrographs using orientation fields. *J. Structural Biology*, 157(2):403 – 415, 2007.
- [16] R. Wang, H. Pokhariya, S. J. McKenna, and J. Lucocq. Recognition of immunogold markers in electron micrographs. *J. Structural Biology*, 176:151–158, 2011.